JCI insight

RESEARCH ARTICLE

Targeting CAR and Nrf2 improves cyclophosphamide bioactivation while reducing doxorubicin-induced cardiotoxicity in triple-negative breast cancer treatment

Sydney Stern,[1] Dongdong Liang,[1] Linhao Li,[1] Ritika Kurian,[1] Caitlin Lynch,[2] Srilatha Sakamuru,[2] Scott Heyward,[3] Junran Zhang,[4] Kafayat Ajoke Kareem,[5] Young Wook Chun,[5] Ruili Huang,[2] Menghang Xia,[2] Charles C. Hong,[5] Fengtian Xue,[1] and Hongbing Wang[1]

[1]Department of Pharmaceutical Sciences, University of Maryland School of Pharmacy, Baltimore, Maryland, USA. [2]National Center for Advancing Translational Science (NCATS), NIH, Rockville, Maryland, USA. [3]Bioreclamation In Vitro Technologies, Halethorpe, Maryland, USA. [4]Department of Radiation Oncology, The Ohio State University James Comprehensive Cancer Center and College of Medicine, Columbus, Ohio, USA. [5]Division of Cardiovascular Medicine, University of Maryland School of Medicine, Baltimore, Maryland, USA.

Cyclophosphamide (CPA) and doxorubicin (DOX) are key components of chemotherapy for triple-negative breast cancer (TNBC), although suboptimal outcomes are commonly associated with drug resistance and/or intolerable side effects. Through an approach combining high-throughput screening and chemical modification, we developed CN06 as a dual activator of the constitutive androstane receptor (CAR) and nuclear factor erythroid 2-related factor 2 (Nrf2). CN06 enhances CAR-induced bioactivation of CPA (a prodrug) by provoking hepatic expression of CYP2B6, while repressing DOX-induced cytotoxicity in cardiomyocytes in vitro via stimulating Nrf2-antioxidant signaling. Utilizing a multicellular coculture model incorporating human primary hepatocytes, TNBC cells, and cardiomyocytes, we show that CN06 increased CPA/DOX-mediated TNBC cell death via CAR-dependent CYP2B6 induction and subsequent conversion of CPA to its active metabolite 4-hydroxy-CPA, while protecting against DOX-induced cardiotoxicity by selectively activating Nrf2-antioxidant signaling in cardiomyocytes but not in TNBC cells. Furthermore, CN06 preserves the viability and function of human iPSC–derived cardiomyocytes by modulating antioxidant defenses, decreasing apoptosis, and enhancing the kinetics of contraction and relaxation. Collectively, our findings identify CAR and Nrf2 as potentially novel combined therapeutic targets whereby CN06 holds the potential to improve the efficacy/toxicity ratio of CPA/DOX-containing chemotherapy.

Introduction

Breast cancer is a heterogeneous malignancy, leading to variable prognoses based on its clinical classification, stage of the disease, and the choice of treatment. In the United States, approximately 290,560 new cases and 43,780 breast cancer–related deaths are estimated in 2022 (1). Triple-negative breast cancer (TNBC) accounts for 10%–20% of all breast cancers and is biologically more aggressive (2). Clinically, TNBC is irresponsive to hormonally targeted therapeutics due to the lack of the expression of estrogen, progesterone, and human epidermal growth factor receptors (3), making conventional chemotherapy the standard of care. Cyclophosphamide (CPA) and doxorubicin (DOX) are 2 key components among the most commonly used chemotherapy regimens for TNBC (4). Although this drug combination improves outcomes of early-stage TNBC, patients with advanced-stage TNBC have markedly lower survival rates. After initial chemotherapy responsiveness, most TNBC patients only achieve a moderate overall pathological complete response while experiencing low therapeutic efficacy and severe adverse drug reactions (5). Thus, there is a critical unmet need to improve CPA/DOX-based therapeutic strategies to achieve greater efficacy against TNBC while minimizing undesirable toxicity.

Conflict of interest: The authors have declared that no conflict of interest exists.

Submitted: August 4, 2021
Accepted: May 10, 2022
Published: May 17, 2022

Reference information: *JCI Insight*. 2022;7(12):e153868. https://doi.org/10.1172/jci.insight.153868.

CPA, a DNA-alkylating prodrug, has a broad spectrum of antineoplastic activity against various types of cancers (6). The therapeutic efficacy of CPA relies largely on metabolic bioactivation to generate the DNA-crosslinking metabolite. Hepatic cytochrome P450 2B6 (CYP2B6) enzyme is predominantly responsible for converting CPA to the intermediate metabolite 4-hydroxycyclophosphamide (4-OH-CPA), the initial and rate-limiting step of CPA bioactivation (7, 8). Other CYP enzymes such as CYP2C9 and CYP3A4 also contribute to this metabolic conversion but to a lesser extent (9, 10). Alternatively, CPA can be metabolized to its inactive metabolite N-dechloroethyl-cyclophosphamide and a toxic byproduct chloroacetyldehyde by CYP3A4 (11). Thus, the therapeutic efficacy of CPA can be potentiated by increasing the expression of CYP2B6, which is transcriptionally regulated by the constitutive androstane receptor (CAR, NR1I3) (12, 13). Previous work in our laboratory has shown that activation of human CAR (hCAR) leads to preferential induction of CYP2B6 over other CYP enzymes and enhances the conversion of CPA to 4-OH-CPA in human primary hepatocytes (HPH) (14, 15).

DOX belongs to the anthracycline class of drugs widely used to treat many types of cancer and is considered highly effective against TNBC in combination with CPA. However, clinical use of DOX is limited by dose-dependent cumulative cardiotoxicity, which can result in cardiomyopathy and congestive heart failure (16). While the precise mechanism of DOX-induced cardiotoxicity remains elusive, conjecture has implicated oxidative stress, mitochondrial dysfunction, impaired ATP levels and calcium metabolism, dysregulation of topoisomerase-IIB, and activation of the ubiquitin protease system (17, 18). Among others, oxidative stress to cardiomyocytes (CM) represents one of the most widely accepted mechanisms underlying DOX-induced cardiotoxicity (19). Oxidative stress occurs when production of reactive oxygen species (ROS) oversaturates the antioxidant defenses of CM. The transcription factor, nuclear factor erythroid 2-related factor 2 (Nrf2), is regarded as the master regulator of the cellular antioxidant response. Upon activation, Nrf2 translocates into the nucleus and stimulates the expression of numerous genes encoding antioxidative, metabolic, and detoxification proteins, and it orchestrates a major cellular defensive mechanism (20, 21). Thus, modulation of the Nrf2-antioxidant signaling in CM may reduce DOX-induced cardiotoxicity.

In this study, we sought to test the hypothesis that dual activation of CAR and Nrf2 enhances the bioactivation of CPA while reducing DOX-mediated cardiotoxicity and improving the efficacy/toxicity ratio of CPA/DOX-based treatment for TNBC. We developed CN06 as a potentially novel hCAR and Nrf2 dual activator and evaluated its potential as an adjuvant to CPA/DOX therapy that would augment anticancer activity while promoting cardioprotection. We also generated a multiorgan coculture system that provides a shared cellular environment including HPH for metabolism, TNBC cells for chemotherapy, and CM as a side-toxicity target. Using this model, we were able to provide proof-of-concept experimental evidence that inclusion of CN06 significantly enhances the anticancer efficacy of CPA while simultaneously alleviating DOX-induced cardiotoxicity, a finding of great potential value for the treatment of TNBC and other cancers responsive to this regimen.

Results

Identification and characterization of CN06 as a dual activator of hCAR and Nrf2. CAR and Nrf2 are transcription factors that control the expression of numerous genes containing xenobiotic response elements with the half-site AGGTCA spaced by 3–6 base pairs and the antioxidant response element (ARE: 5′-TGACXXXGC-3′) in their regulatory regions, respectively (22, 23). Using a hCAR high-throughput screening (HTS) luciferase assay developed in our lab previously (24), we initially screened a collection of chemicals including 5632 compounds from the NCATS Pharmacologically Active Chemical Toolbox (NPACT) library and 277 synthesized compounds from an in-house University of Maryland Baltimore (UMB) library. As illustrated in Figure 1A, this screening led to the identification of 468 compounds as potential hCAR activators when the criteria of potency (EC_{50} < 20 μM) and efficacy (E > 50% of the positive control) were applied. These hits were subsequently subjected to a Nrf2 activation assay as described previously (25). The combined approach resulted in the identification of 43 potential dual activators of hCAR and Nrf2 (Figure 1A and Supplemental Table 1; supplemental material available online with this article; https://doi.org/10.1172/jci.insight.153868DS1). Further evaluation of the top 20 dual activators revealed that compound CN06 exhibited the most robust induction of hepatic CYP2B6 (Figure 1B) and cardiac heme oxygenase-1 (HO-1; Figure 1C), the prototypical target genes for hCAR and Nrf2, respectively.

Structurally, CN06 falls into the group of synthetic compounds designed by hybridizing our previously reported imidazothiazole-based hCAR activator DL5016 (26) with the Nrf2 activating group, an isothiocyanate (NCS, Figure 1D) and demonstrated optimal activation of both hCAR and Nrf2 compared with its

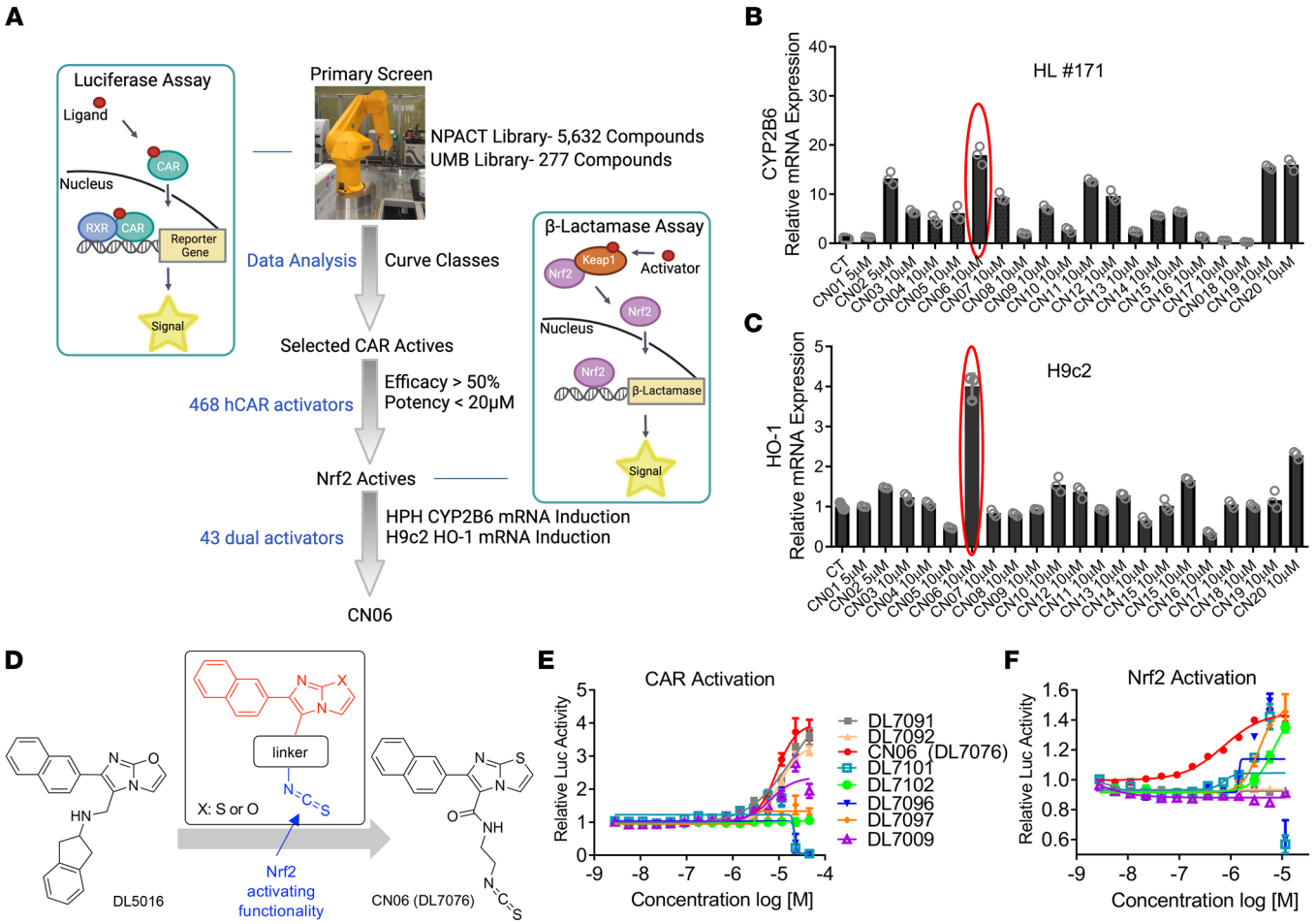

Figure 1. Cell-based high-throughput screening and identification of dual activators of hCAR and Nrf2. Human CAR luciferase activity assay was used to screen the NPACT (5632 compounds) and a UMB (277 compounds) libraries. (**A**) Compounds (468) meeting the criteria of EC_{50} < 20 μM and efficacy > 50% of the positive control were subjected to a β-lactamase assay (Nrf2 activity), leading to the identification of 43 promising candidates of hCAR/Nrf2 dual activators. (**B** and **C**) The top 20 hCAR/Nrf2 dual activators were tested using RT-PCR for their potential induction of CYP2B6 in cultured human primary hepatocytes (**B**) and of HO-1 in H9c2 cells (**C**). (**D**) Chemical features of the CN06 (DL7076) class re illustrated. (**E** and **F**) Luciferase activity assays for the activation of CAR (**E**) and Nrf2 (**F**), respectively, by 8 CN06 analogues were measured at indicated concentrations. Data are expressed as mean ± SD from 3 experiments. HL#171, primary hepatocytes prepared from human liver donor #171.

synthetic analogues (Figure 1, E and F, and Supplemental Figure 1). At concentrations that markedly activate hCAR and Nrf2, and induce their target genes, CN06 is nontoxic to HPH, TNBC cells, H9c2 cells, or human iPSC–derived CM (hiPSC-CM; Supplemental Figure 2). Based on these findings, we tested CN06 as a proof-of-concept model dual activator of hCAR/Nrf2 in subsequent studies.

CN06 induces hepatic expression of CYP2B6 over CYP3A4 via activation of hCAR. CYP2B6 is a highly inducible hepatic drug-metabolizing enzyme that is transcriptionally regulated by hCAR, while — to a lesser extent — by the pregnane X receptor (PXR) (27). Activation of hCAR preferentially induces hepatic expression of CYP2B6, while PXR activation favors the induction of CYP3A4 (28, 29). To examine whether the newly developed hCAR/Nrf2 dual activator preferentially induces CYP2B6 expression, we treated HPH from multiple liver donors with CN06 (donor demographics in Supplemental Table 2). CN06 markedly induced the expression of CYP2B6 mRNA and protein in a concentration-dependent manner, with negligible induction of CYP3A4 (Figure 2, A–F). Activation of PXR by rifampicin (RIF), as expected, led to robust induction of CYP3A4. Nuclear translocation of CAR in hepatocytes is an important first step of chemical-induced CAR activation (30). Previously, we showed that adenovirus expressing enhanced yellow fluorescent protein–tagged (EYFP-tagged) hCAR (Ad/EYFP-hCAR) infects HPH with high efficiency and that chemical-mediated Ad/EYFP-hCAR nuclear translocation in HPH correlates with hCAR activation and target gene expression (31–33). As shown in Figure 2G, CN06 markedly translocated hCAR from the cytoplasm to the nucleus at a

concentration that displays robust CYP2B6 induction in HPH. Phenobarbital (PB), a known hCAR activator, served as a positive control. Together, these results indicate that CN06 can activate hCAR in HPH, leading to preferential induction of CYP2B6 over CYP3A4 expression.

Given the favorable effects of CYP2B6 on CPA 4-hydroxylation and bioactivation, we next examined the potential effects of CN06 on the bioactivation and anticancer activity of CPA using an HPH-TNBC cell coculture model as depicted in Figure 2H. Our results show that, in comparison with CPA treatment alone, cotreatment of CPA with CN06 significantly reduced the cell viability of BT549, a TNBC cell line (Figure 2I). Notably, in the presence of CN06 (10 μM), CPA at 250 μM markedly increased cell death in BT549 cells similar to that observed with 1000 μM CPA alone. To further evaluate the effects of CN06 on CPA bioactivation, the culture medium from each treatment condition was collected for liquid chromatography–tandem mass spectrometry (LC-MS/MS) quantification of 4-OH-CPA. As shown in Figure 2J, coexposure of CN06 with CPA at multiple concentrations significantly increased the formation of 4-OH-CPA in the culture medium. These results indicate that CPA-mediated cytotoxicity in TNBC cells can be enhanced through hCAR-mediated augmentation of hepatic 4-OH-CPA formation by CN06.

CN06 activates Nrf2 antioxidant signaling in H9c2 cells but not in TNBC cells. A dose-limiting side effect of DOX is cardiotoxicity caused by oxidative stress in CM. Nrf2 is considered a master cytoprotective factor that regulates the expression of genes encoding antioxidant, antiinflammation, and detoxification proteins (20). Among others, *HO-1* is a prototypical Nrf2 target gene that protects cells against oxidative stress (34). Activation of Nrf2/HO-1 antioxidant signaling has been considered a promising mechanism to counter DOX-induced cardiac oxidative damage. To evaluate the effects of CN06 on the activation of Nrf2 and expression of HO-1, we employed an embryonic rat CM line (H9c2 cells), broadly used as an in vitro model to study drug-induced cardiotoxicity. Our data show that CN06 concentration-dependently induced the expression and nuclear accumulation of Nrf2 in H9c2 cells (Figure 3A), which led to the induction of *HO-1* mRNA and protein (Figure 3B). In contrast, CN06 only marginally altered HO-1 mRNA expression in MDA-MB-231 and BT549 TNBC cells (Figure 3, C and D) and had no influence on HO-1 and Nrf2 protein expression in these 2 TNBC cell lines (Figure 3, E and F). Although the molecular mechanisms by which CN06 activates Nrf2/HO-1 signaling in H9c2 cells, but not in TNBC cells, are unclear, we observed that the endogenous basal levels of Nrf2 in TNBC cells are markedly higher than that in CM (Supplemental Figure 3). Collectively, these results indicate that CN06 activates Nrf2/HO-1 antioxidant signaling in a cell-specific manner and has the potential to protect against DOX-induced cardiotoxicity without simultaneously augmenting chemoresistance in the targeted TNBC cells.

CN06 attenuates DOX-induced cell death in H9c2 but not in TNBC cells. Induction of DNA damage and apoptosis is a major pharmacological action of DOX in cancer cells, while it is a key safety concern in off-target cells (35). To investigate the protective effects of Nrf2 activation on DOX-induced cardiotoxicity, H9c2 cells were pretreated with vehicle control and CN06 at 1, 5, or 10 μM for 2 hours, followed by cotreatment combinations with/without DOX (2.5 μM) for 24 hours. No cell death was observed with CN06 alone at these concentrations, in comparison with vehicle control. In contrast, in line with previous reports (36, 37), 2.5 μM DOX alone reduced H9c2 cell viability by approximately 60% (Figure 4A). Notably, the DOX-induced cell death in H9c2 cells was reversed by CN06 in a concentration-dependent manner; 10 μM CN06 rescued CM viability to ~80% of vehicle control (Figure 4A). These results were confirmed using another cell viability assay (Cell Titer Glo; Supplemental Figure 4). Western blotting analysis revealed that DOX markedly repressed Nrf2 and HO-1 expression, while it augmented the level of cleaved caspase 3 in H9c2 cells and, importantly, these DOX-induced alterations were concentration-dependently reversed in the presence of CN06 (Figure 4B). In a separate experiment using MDA-MB-231 and BT549 cells under the same treatment scheme, CN06 did not affect DOX-induced cell death in either MDA-MB-231 or BT549 cells (Figure 4, C and D). In parallel with the cytotoxic responses, CN06 alone did not significantly induce the expression of Nrf2, HO-1, or cleaved caspase 3, nor did it alter the expression of these proteins when cotreated with DOX in the TNBC cells (Figure 4, E and F). Additionally, CN06 protection of DOX-induced cell death, apoptosis, and DNA damage was observed in 3D spheroid cultures of H9c2 but not BT549 cells (Supplemental Figures 5 and 6). Collectively, our findings indicate that CN06 protects against DOX-induced cardiotoxicity without compromising its anticancer activity in TNBC cells.

CN06 selectively reduces DOX-induced generation of ROS in H9c2 cells. Oxidative stress and the modulation of mitochondrial ROS are important mechanisms through which DOX asserts its cardiotoxicity (38). In this experiment, we aimed to examine DOX-induced oxidative stress in H9c2 CM and the impact of

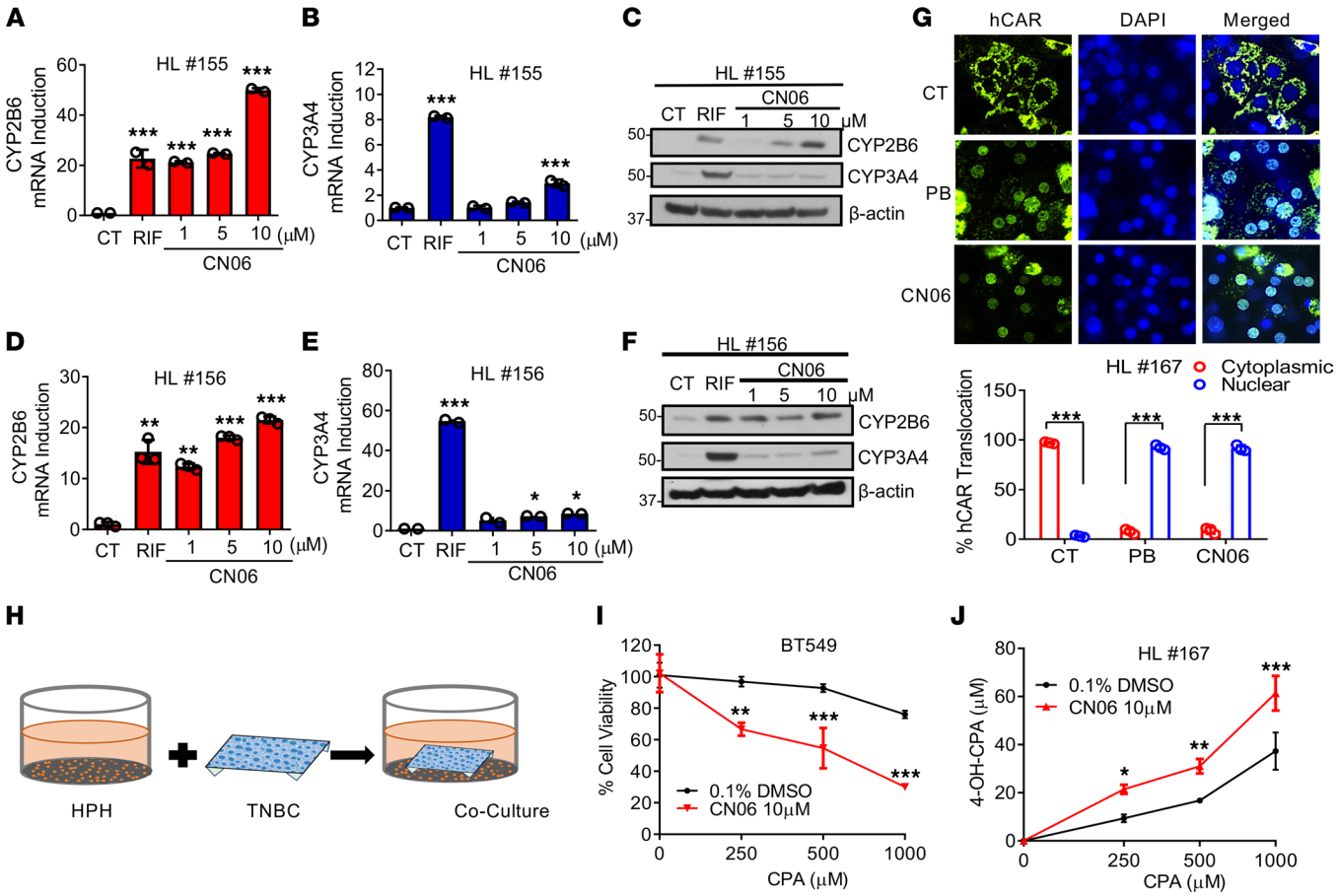

Figure 2. CN06 induces CYP2B6 expression via CAR activation, enhances CPA conversion to 4-OH-CPA, and reduces TNBC cell viability. (**A**–**F**) HPH prepared from liver donors (HL#155; **A**–**C**) and HL#156; **D**–**F**) were treated with vehicle control (0.1% DMSO), RIF (10 μM), and CN06 (1 μM, 5 μM, and 10 μM). The expression of CYP2B6 and CYP3A4 was measured using RT-PCR and Western blotting. PCR data represent mean ± SD, $n = 3$ (analyzed with 1-way ANOVA). (**G**) Cultured HPH (HL#167) were infected with Ad/EYFP-hCAR and treated with vehicle control (0.1% DMSO), PB (1 mM), or CN06 (10 μM) for 8 hours before fluorescence microscopy visualization of EYFP-hCAR localization. Approximately 100 FYFP-hCAR expressing cells from each well and 3 wells from each group were counted for the subcellular localization of hCAR and analyzed using a 2-tailed Student's *t* test. (**H**) Schematic illustration of the coculture model containing HPH and BT549 cells. (**I**) In the coculture model, CPA-induced cell death in BT549 cells was measured after 24-hour cotreatment with/without CN06 (10 μM) ($n = 3$, data represent mean ± SD, 2-way ANOVA with Bonferroni post hoc). (**J**) Concentration-dependent conversion of CPA to 4-OH-CPA was analyzed using LC-MS/MS from the culture medium in the presence and absence of CN06. Results are expressed as mean ± SD ($n = 3$). Statistical significance was determined at $^*P < 0.05$, $^{**}P < 0.01$, $^{***}P < 0.001$. Original magnification ×10.

coadministering CN06. CellROX Green (Thermo Fisher Scientific) is a cell-permeable probe that, upon entering cells, is oxidized by ROS and subsequently binds to DNA to produce a lasting fluorescence signal. As shown in Figure 5A, DOX concentration-dependently increased ROS generation in H9c2 cells, whereas this DOX-induced ROS accumulation was significantly repressed by CN06. As suggested by the results of experiments described above, CN06 favors CM protection by activating the Nrf2/HO-1 antioxidant pathway. We next assessed the production of ROS in the TNBC cell lines (MDA-MB-231 and BT549). Under the same treatment conditions, DOX significantly induced ROS production in both MDA-MB-231 and BT549 cells, and notably, this was not altered when CN06 was added (Figure 5, B and C). These results support the conclusion that including CN06 decreased DOX-mediated ROS generation in H9c2 CM, but not in targeted TNBC cells.

CN06 enhances the anticancer activity while repressing cardiotoxicity of the CPA/DOX combination in a multicellular coculture model. We next evaluated the potential that inclusion of the hCAR/Nrf2 dual activator, CN06, in the CPA/DOX combination improves anticancer efficacy while decreasing off-target cardiotoxicity. As depicted in Figure 6A, we developed a multicellular coculture model containing HPH, TNBC cells, and CM. Results from cell viability assays showed that CN06 significantly increased CPA/DOX-mediated cell death in BT549 cells (Figure 6B), while protecting H9c2 cells (Figure 6C) from the chemotherapeutic

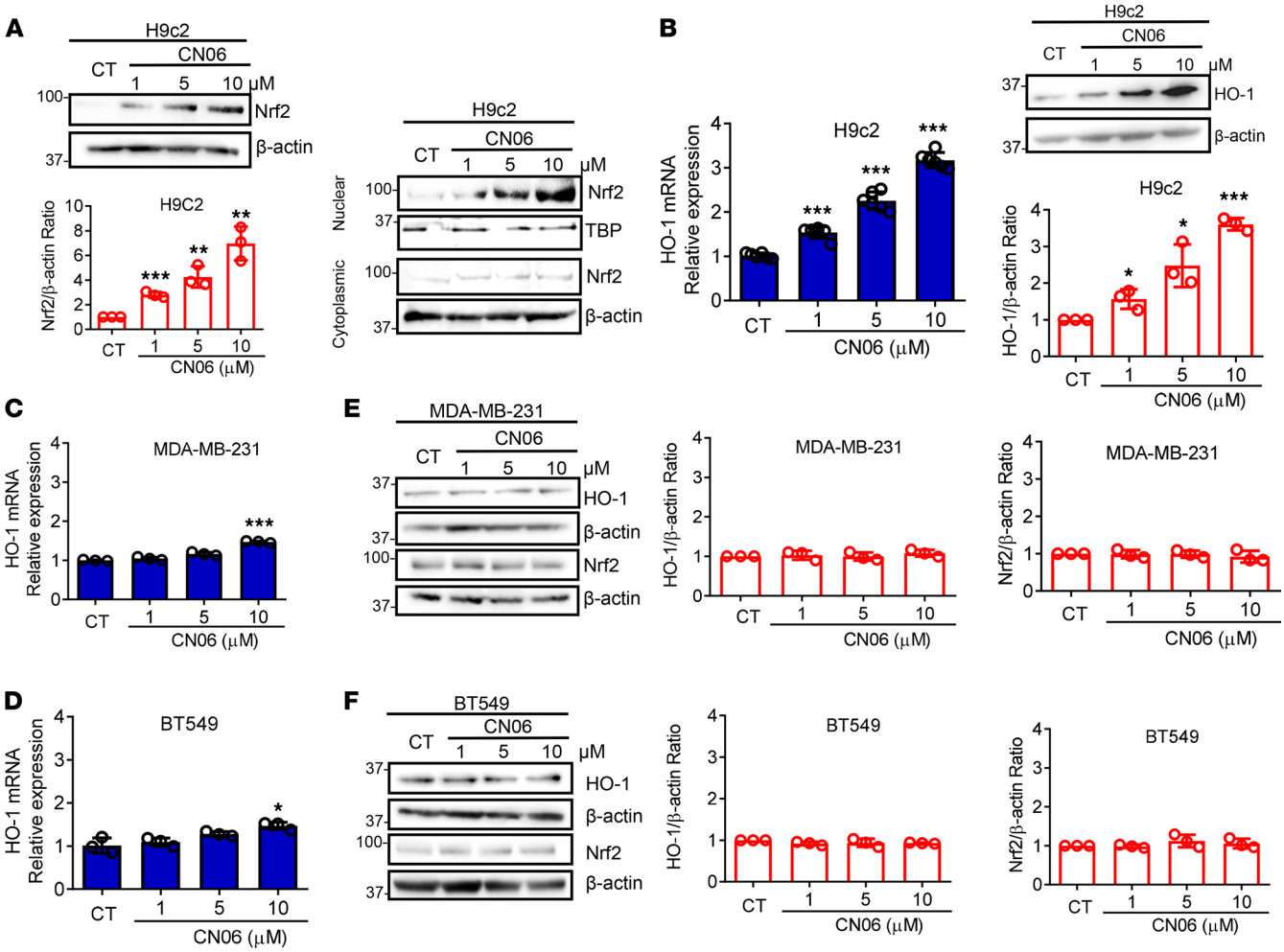

Figure 3. CN06 activates Nrf2 and induces HO-1 in a tissue preferential manner. H9c2 cells were treated with vehicle control (0.1% DMSO) or CN06 at 1 μM, 5 μM, and 10 μM for 24 hours. (**A**) Expression of Nrf2 in whole cell lysate, cytoplasm, and nuclear extracts was analyzed using Western blotting. β-Actin and TBP were used as loading controls for cytosol and nuclear extracts, respectively. (**B**) mRNA and protein of HO-1 were measured by RT-PCR and Western blotting (n = 3, data represent mean ± SD, 1-way ANOVA with Bonferroni post hoc). In separate experiments, MDA-MB-231 and BT549 cells were treated with vehicle control or CN06 as indicated above. (**C**–**F**) Expression of HO-1 mRNA (**C** and **D**) and protein of HO-1 and Nrf2 (**E** and **F**) was analyzed using RT-PCR and Western blotting, respectively. Results are expressed as fold over control, mean ± SD (n = 3). Densitometry was quantified as a ratio of protein-of-interest/β-actin using ImageJ from 3 independent experiments. One-way ANOVA with a Bonferroni post hoc was performed. Statistical significance was determined at $^{*}P < 0.05$,$^{**}P < 0.01$, $^{***}P < 0.001$.

agents in the multicellular microenvironment. At this concentration range, CPA/DOX combination had a negligible impact on HPH viability with or without CN06 cotreatment (Supplemental Figure 7).

Phosphorylation of histone H2A variant H2AX at Ser139 (γ-H2AX) is a sensitive marker for DNA double-stranded breaks induced by many chemotherapeutics including the CPA/DOX combination (39). In our coculture experiments, we found that, compared with CPA/DOX treatment alone, CN06 significantly enhanced CPA/DOX-induced phosphorylation of H2AX (γ-H2AX) in BT549 cells (Figure 6, D and E). Notably, in the same coculture system, CN06 markedly attenuated the level of γ-H2AX in the cocultured H9c2 cells (Figure 6, F and G). Collectively, these data are consistent with the observed cell-specific regulation of hCAR/CYP2B6 and Nrf2/HO-1 pathways by CN06 and support the notion that combining a hCAR/Nrf2 dual activator with a CPA/DOX-containing chemotherapy regimen against TNBC can enhance anticancer activity while attenuating cardiotoxicity.

CN06 protects DOX-induced cell death and contractility in hiPSC-CMs. Properly cultured hiPSC-CMs have emerged as a promising in vitro disease-relevant model for studying drug-induced cardiotoxicity. Two colonies of hiPSC-CMs generated by a chemically defined differentiation protocol were used to test the effects of CN06 on DOX-induced cardiotoxicity. As shown in Figure 7A, the hiPSCs used were

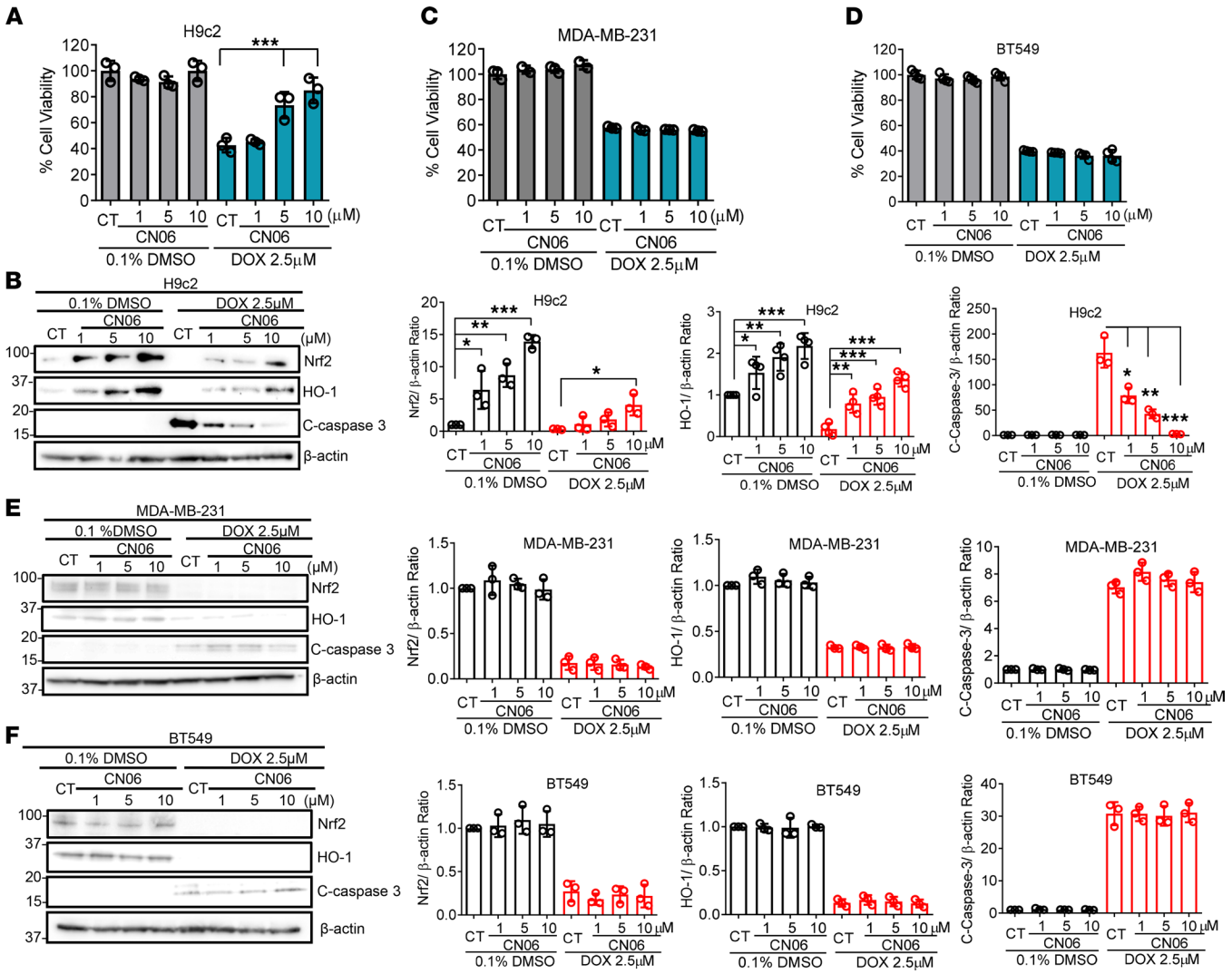

Figure 4. CN06 protects DOX-induced cell death in H9c2 cells but not in TNBC cells. Cultured H9c2, MDA-MB-231, and BT549 cells were pretreated with vehicle control (0.1% DMSO) or CN06 (1 μM, 5 μM, 10 μM) for 2 hours, followed by CN06 with/without DOX (2.5 μM) for 24 hours. (**A**, **C**, and **D**) Cell viability was measured using a CCK-8 kit following the manufacturer's instructions in treated H9c2 (**A**), MDA-MB-231 (**C**), and BT549 (**D**) cell lines, respectively (n = 3, data represent mean ± SD, 1-way ANOVA with Bonferroni post hoc). (**B**, **E**, and **F**) Expression of Nrf2, HO-1, and cleaved caspase 3 was measured by Western blotting using whole cell lysates isolated from treated H9c2 (**B**), MDA-MB-231 (**E**), and BT549 (**F**) cells. RT-PCR results are expressed as fold over control, mean ± SD (n = 3). For Western blotting, band densitometry was quantified as a ratio of protein-of-interest/β-actin using ImageJ from 3 independent experiments. Data were analyzed using 1-way ANOVA with Bonferroni post hoc. Statistical significance was determined at $^*P < 0.05$,$^{**}P < 0.01$, $^{***}P < 0.001$.

confirmed to contain pluripotency by immunostaining of Oct4 and TRA-60α, and the validated hiPSCs were successfully differentiated into hiPSC-CMs with positive staining of cardiac α-actinin. Using these hiPSC-CMs, we demonstrated that CN06 concentration-dependently induced the expression of *HO-1* mRNA (Figure 7B), as well as HO-1 and Nrf2 protein levels (Figure 7C). Treatment with 2.5 μM DOX reduced the viability of hiPSC-CMs, and importantly, CN06 markedly rescued hiPSC-CMs from DOX-induced cell death (Figure 7D and Supplemental Figure 8). Consistent with the cytotoxicity findings, CN06 reversed DOX-mediated suppression of Nrf2 and HO-1 expression, as well as its induction of cleaved caspase 3 in hiPSC-CMs (Figure 7E). Functionally, by impairing hiPSC-CM contractility, DOX (1 μM) treatment significantly reduced cell shortening compared with vehicle control or CN06 alone (Figure 7F). Notably, DOX-induced impaired cell shortening was efficiently rescued by adding CN06 (Figure 7F). Moreover, cardiac α-actinin staining revealed that DOX-impaired sarcomere organization in hiPSC-CMs was partially rescued by CN06 (Supplemental Figure 9). Collectively, these results suggest that CN06 can preserve the viability and function of hiPSC-CMs by modulating the

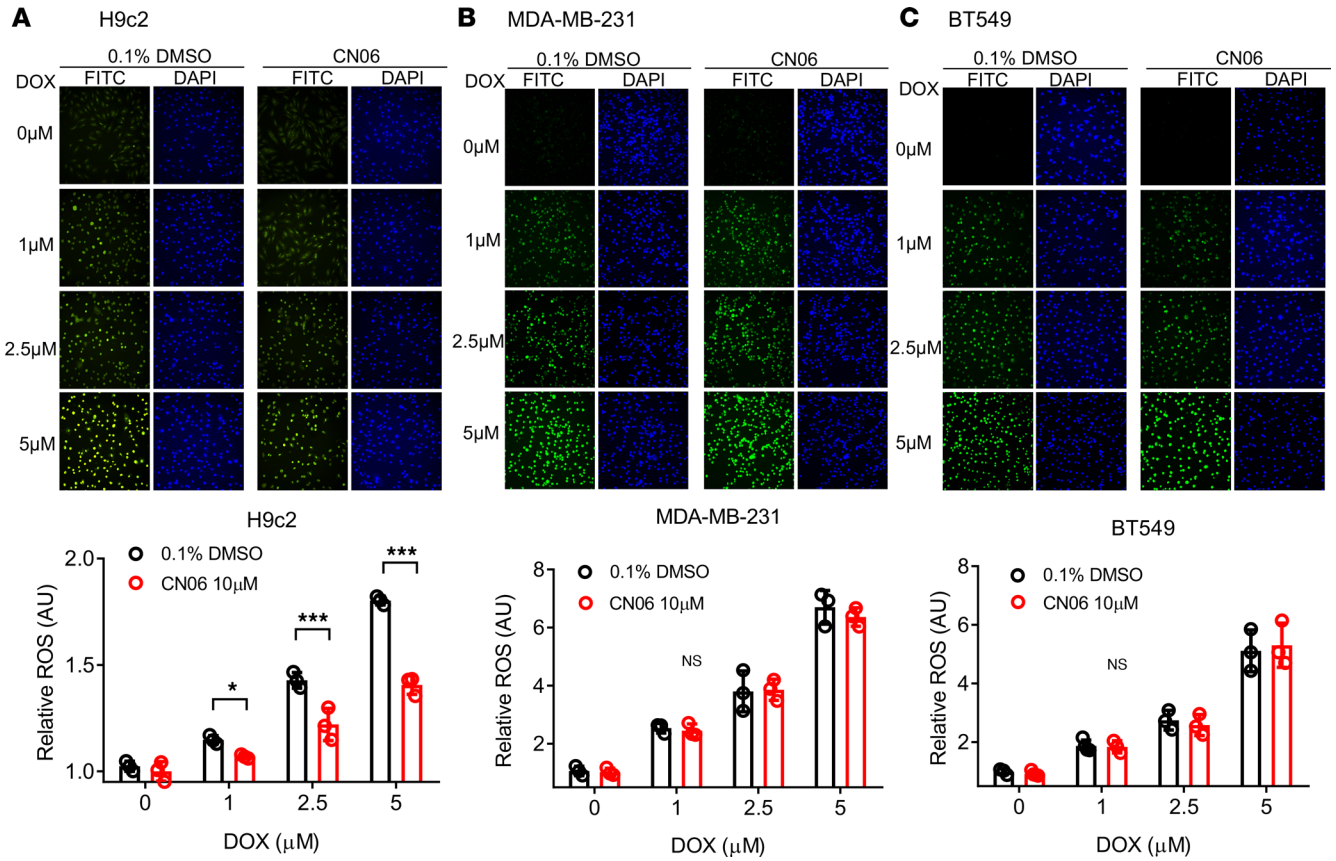

Figure 5. CN06 reduces DOX-induced reactive oxygen species (ROS) production in H9c2 but not TNBC cells. Cultured H9c2, MDA-MB-231, and BT549 cells were pretreated for 2 hours with 0.1% DMSO or CN06 (10 μM) and then cotreated with DOX at 1, 2.5, and 5 μM for 6 hours. ROS content was assessed by adding 5 μM Cell ROX Green at 37°C and 5% CO_2 for 30 minutes. The fluorescence was quantified as a mean integrated intensity using NIS-Element Analysis with bright-spot detection and normalized to the vehicle control. (**A**–**C**) Representative images via fluorescence microscopy were shown for treated H9c2 (**A**), MDA-MB-231 (**B**), and BT549 (**C**). Relative ROS production was quantified from 3 wells per group. Data represent mean ± SD, One-Way ANOVA with Bonferroni post hoc. Statistical significance was determined by vehicle control versus treatment group at $^*P < 0.05$, $^{***}P < 0.001$. Original magnification ×10.

antioxidant defense, decreasing apoptosis, and enhancing the kinetics of contraction and relaxation. Our findings support the therapeutic potential of CN06, as a dual activator of CAR/Nrf2, to enhance the efficacy/toxicity ratio of CPA/DOX-based chemotherapy for TNBC (Figure 7G).

Discussion

Lack of known targeted therapies greatly impedes the treatment of TNBC, leaving traditional cytotoxic chemotherapy as the mainstay of management. Currently, many chemotherapy regimens for TNBC contain CPA and DOX as key components; however, these approaches are often associated with subpar clinical outcomes and off-target cardiotoxicity. In this work, we have developed CN06 as a representative dual activator of hCAR and Nrf2, which simultaneously enhances hCAR-mediated CYP2B6 expression and CPA bioactivation, while reducing DOX-induced cardiotoxicity through activation of Nrf2 antioxidant signaling in CM but not in TNBC cells. These findings reveal hCAR and Nrf2 as potentially novel combined therapeutic targets, and dual activation of these receptors represents a possible strategy to improve the therapeutic window of CPA/DOX-based chemotherapy.

CN06 is a chemical hybrid built upon the structural backbone of our previous hCAR activator DL5016 and an isothiocyanate group, a key functionality found in several Nrf2 activators. While further chemical optimization is warranted, CN06 exhibits robust activation of both hCAR and Nrf2 in comparison with its synthetic analogs, as well as the hits from screening of the NPACT and UMB libraries. In HPH culture, we found that CN06 preferentially induced the expression of CYP2B6 over CYP3A4 and efficiently translocated hCAR from the cytoplasm to the nucleus of hepatocytes, suggesting that CN06 maintains the key characteristic of its parent DL5016 in hCAR activation. Indeed, such a feature allowed CN06 to enhance the bioactivation of CPA

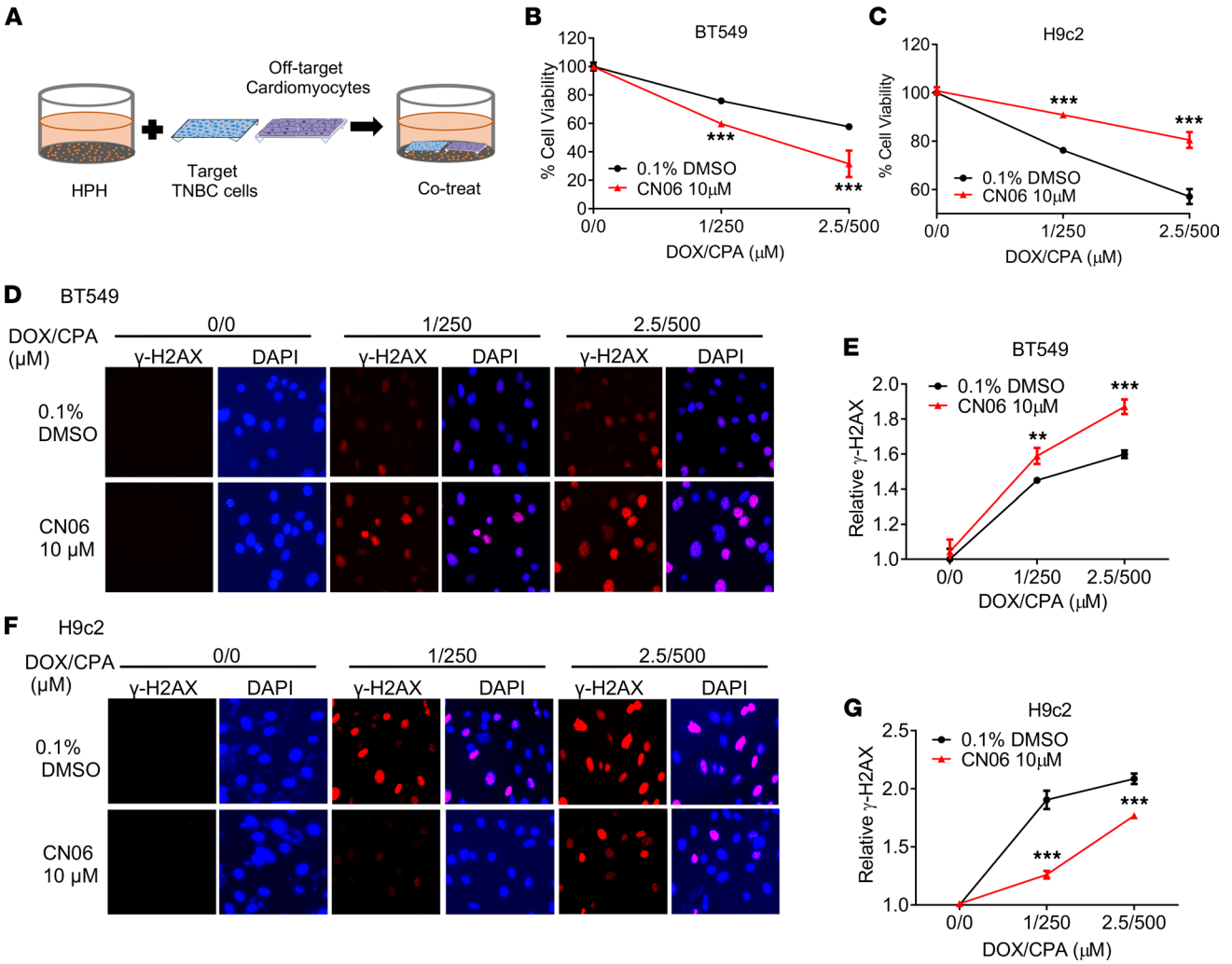

Figure 6. CN06 enhances cell death in BT549 cells while protecting H9c2 cells treated with the DOX/CPA combination in a multicellular coculture model. (**A**) Schematic illustration of the multicellular coculture model containing BT549 cells, H9c2 cardiomyocytes, and HPH. (**B** and **C**) In the coculture model, CPA/DOX-induced cell death in BT549 (**B**) and H9c2 (**C**) cells was measured in the presence and absence of CN06 (10 μM), respectively (n = 3, data represent mean ± SD, 2-way ANOVA with Bonferroni post hoc). (**D** and **F**) Treated BT549 (**D**) and H9c2 (**F**) cells were removed from the coculture system and fixed with 4% paraformaldehyde, followed by an immunostaining for H2AX phosphorylated at serine-139 position of histone (γ-H2AX). (**E** and **G**) Relative γ-H2AX signal was quantified using NIS-Element Analysis using bright-spot detection and normalized to the vehicle control. FITC channel was modified to red for readers' clarity, and DAPI staining of nucleus was in blue. Three whole-well images from each group were used for signal quantification. Data were analyzed using a 2-way ANOVA with a Bonferroni post hoc. Representative images via fluorescence microscopy are shown. All values are presented as fold change versus treatment control. Statistical significance was determined at $^{**}P < 0.01$, $^{***}P < 0.001$. Original magnification ×10.

and its anticancer activity in TNBC cells cocultured with HPH. During systemic therapy, the active metabolite, 4-OH-CPA, generated in the liver, was subsequently exported to extrahepatic tissues via circulation (40). It is noteworthy that, while most CPA therapeutic targets are extrahepatic malignancies, metabolic conversion of CPA to 4-OH-CPA is completed predominantly in the liver, with hepatic CYP2B6 as the rate-limiting enzyme (41). The endogenous expression of CYP2B6 and CAR in many extrahepatic cancers (14), including breast cancer, is extremely low (Supplemental Figure 10), and in situ bioactivation of CPA in these malignant cells is inconsequential. Thus, it is perhaps not surprising that simply increasing the dose of CPA in cancer patients as reported previously lacked significant benefit (42). Most recently, we showed that hepatic induction of CYP2b10 (the murine analog of human CYP2B6) is sufficient to improve CPA-based treatment of lymphoma xenografts in mice (43), suggesting that manipulation of CYP-mediated activation of CPA in the liver represents a logical approach to enhance CPA-based chemotherapy.

To date, while the clinical benefit of combining CPA and DOX in TNBC treatment has been well documented, DOX-induced cardiotoxicity remains a major safety concern that can lead to early termination of

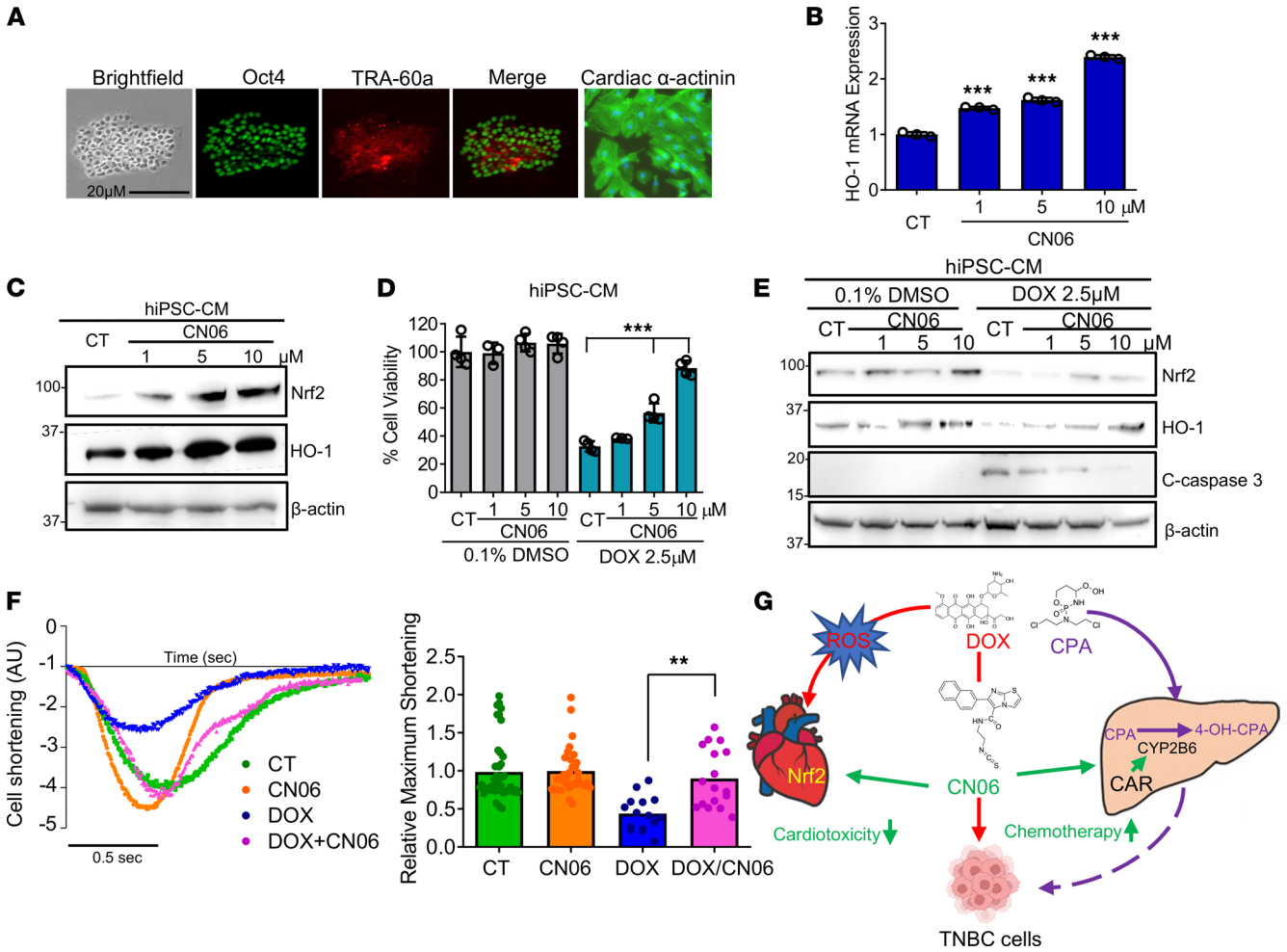

Figure 7. CN06 protects DOX-induced cell death and impaired contractility in hiPSC-CMs. (**A**) Immunostaining of Oct4 and Tra-60α for the pluripotency of hiPSC, and cardiac α-actinin for the pluripotency of hiPSC-CMs. Differentiated hiPSC-CMs were treated with 0.1% DMSO (CT), or CN06 at 1, 5, and 10 μM for 24 hours. (**B** and **C**) RT-PCR was used to analyze HO-1 mRNA expression (**B**), and Western blotting was used to detect the protein expression of HO-1 and Nrf2 (**C**) (n = 3, data represent mean ± SD, 1-way ANOVA with a Bonferroni post hoc). In separate experiments, hiPSC-CMs were pretreated with vehicle control or CN06 (1, 5, and 10 μM) for 2 hours, followed by a cotreatment with/without DOX (2.5 μM) for another 24 hours. (**D**) Cell viability was determined using CCK8 reagent. (**E**) Protein expression of Nrf2, HO-1, and cleaved caspase 3 under the same treatment condition was analyzed using Western blotting. To detect cell contractility, hiPSC-CMs were cultured in the presence of vehicle control or CN06 (10 μM) for 24 hours, followed by a 6-hour cotreatment with DOX (1 μM). (**F**) Video-based edge detection was used to assess cellular shortening of the hiPSC-CMs during spontaneous contraction (n = 20–35 single cells, data represent mean ± SD, 2-tailed Student's t test). Analyses of traces were completed using the instrument packaged IonWizard v7.3 data analysis software. (**G**) The beneficial effects of CN06 as a dual activator of CAR/Nrf2 on CPA/DOX-based treatment of TNBC were depicted in a schematic illustration. All values are normalized to the vehicle control. Statistical significance was determined at $^{**}P < 0.01$, $^{***}P < 0.001$.

treatment or heart failure. It has been estimated that more than 10% of patients treated with DOX or its derivatives developed cardiac complications (44). The need to prevent and treat DOX-mediated cardiotoxicity in cancer survivors remains challenging. Dexrazoxane, an iron-chelating agent, is the only FDA-approved drug specifically indicated to prevent DOX-induced cardiomyopathy. However, it is associated with substantial safety concerns (18). We show that, in addition to enhancing CPA bioactivation, CN06 markedly attenuates DOX-induced ROS generation, apoptosis, and DNA damage in CM by activating Nrf2 antioxidant signaling, a widely acknowledged mechanism by which cells protect themselves from toxic chemicals that produce oxidative and electrophilic stresses. Our findings are consistent with previous reports in which DOX-induced cardiotoxicity was attenuated through the activation of Nrf2 by compounds such as sulforaphane, an isothiocyanate-containing compound isolated from broccoli (45), or by miR-200a–mediated degradation of Kelch-like ECH-associated protein 1 (KEAP1), a key repressor protein that promotes Nrf2 degradation (46).

It is widely accepted that activation of Nrf2 upregulates a cluster of genes that encode cytoprotective proteins important to antioxidant response and detoxification. This, however, could be a double-edged

sword where, on one hand, activation of Nrf2 protects normal cells against oxidative stress and other toxic challenges, while on the other hand, aberrant Nrf2 activation in cancer cells provokes malignant growth and anticancer drug resistance (47). Therefore, whether Nrf2 activators can serve as a suitable therapeutic approach relies largely on its tissue selectivity. Importantly, our data demonstrate that compound CN06 markedly activates Nrf2 and induces its target gene expression in CM with negligible effects on Nrf2 signaling in TNBC cells. Moreover, the preferential activation of Nrf2 antioxidant signaling in CM led to selective protection of DOX-induced cardiotoxicity without sacrificing its chemotherapeutic effects on TNBC cells. Of note, while the mechanism underlying the selective Nrf2 activation by CN06 is yet to be elucidated, accumulating evidence reveals that somatic mutations in KEAP1 or Nrf2 genes result in constitutive Nrf2 activation in many cancers, including TNBC (48). Indeed, we found that basal expression of Nrf2 in TNBC cell lines is markedly higher than that in CM and HPH (Supplemental Figure 3). Therefore, we speculate that the high basal expression and constitutive activation of Nrf2 in TNBC cells over CM contribute to the observed preferential protection of CN06 against DOX-induced cardiotoxicity.

Currently, most in vitro evaluation of the pharmacological properties of chemotherapeutics utilizes immortalized cancer cell lines without adequately considering the influences of hepatic metabolism and off-target toxicity that affect the therapeutic efficacy and safety of drugs. In particular, cancer cells often express low levels of drug-metabolizing enzymes and only play a moderate role in the metabolism and bioactivation of anticancer drugs in situ. In this study, we used a multicellular coculture model incorporating HPH, TNBC cells, and CM, which enables synchronous investigation of the chemotherapeutic effects of CPA/DOX on TNBC and the toxic side effects on CM with and without CN06, in a multicellular environment where hepatic metabolism is well maintained. We found that CN06 concurrently increases CPA/DOX-mediated DNA damage and cell death in TNBC cells, while rescuing these cell damages in the cocultured CM. Notably, CN06 facilitates CPA/DOX-based TNBC treatment by targeting 2 independent signaling pathways in a cell-specific manner, and the multicellular coculture system appears to be a valuable model for in vitro evaluation of the efficacy and toxicity of CPA/DOX-based chemotherapy.

To this end, our cardiotoxicity data were generated using the H9c2 line of embryonic rat CM. Despite its easy culture, rapid amplification, and as an in vitro CM model broadly used for studying drug-induced cardiotoxicity, H9c2 cells do not exhibit cardiac functions such as spontaneous rhythmic contractions and are not of human origin. Properly cultured hiPSC-CMs represent a promising in vitro human-relevant model for studying drug-induced cardiotoxicity. We found that DOX markedly reduced the contractibility and viability of hiPSC-CMs, and this information is in agreement with previous reports (49, 50). Clearly treatment duration, metabolic stress, and maturation of hiPSC-CMs contribute to the degree of toxic responses. Concerns raised by a recent report indicate that the metabolic selection method may mimic ischemic conditions, upon analysis being carried out within 4 days of metabolic selection (51). In contrast, we performed our phenotype characterization after culturing hiPSC-CMs in glucose-containing medium for 15–20 days, a timeframe during which these cells are presumed to have recovered from metabolic stress. Consistent with observations in H9c2 cells, treatment with CN06 effectively rescued DOX-induced cardiotoxicity in hiPSC-CMs, which is associated with increased expression of Nrf2 and its target gene *HO-1*. Furthermore, at the single-cell level, DOX-suppressed hiPSC-CMs contractility was remarkably alleviated by CN06.

Collectively, our results highlight dual activation of hCAR and Nrf2 by CN06 as a promising approach to advance CPA/DOX-based chemotherapy of TNBC via hCAR-mediated CYP2B6 induction and CPA bioactivation, as well as Nrf2-dependent cardioprotection against DOX. Intriguingly, the tissue-selective modulation of Nrf2 activity by CN06 confers cardioprotection without desensitizing the antitumor effect of DOX in TNBC cells. Of note, our multicellular coculture model appears to be effective in concomitant investigation of hepatic metabolism, cancer treatment, and off-target cardiotoxicity. One limitation of the current study, however, is the lack of in vivo animal experiments due to insufficient CN06 solubility. Further optimization of CN06 to improve its druggable features, including the pharmacokinetic, pharmacodynamic, and toxicological profiles, is warranted. In addition, recent reports indicated that persistent activation of Nrf2 signaling may lead to myocardial damage and dysfunction, an emerging dark side of Nrf2 in heart (52). Therefore, more detailed studies are required to illustrate whether CN06 provokes the dark side of Nrf2 in vivo and to determine the safety and efficacy of CN06 or its analog as an adjuvant to CPA/DOX-containing regimens in mammalian models. Nevertheless, CN06 is the first compound to our

knowledge developed to specifically target both the hCAR-CYP2B6 and Nrf2-antioxidant pathways and to exhibit proof-of-concept results supporting dual activation of hCAR and Nrf2 as a potential approach to benefit patients receiving CPA/DOX-based regimens.

Methods

Supplemental Methods are available online with this article.

Chemicals and biological reagents. CPA, DOX, semicarbazide hydrochloride (SCZ), DAPI, PB, DMSO, RIF, and 2',7'-dichlorofluorescein diacetate (DFDA) were purchased from Sigma-Aldrich. Cell Rox Green was obtained from Thermo Fisher Scientific. CN06 and its analogues were synthesized and purified as described elsewhere (26). Oligonucleotide primers were synthesized by Integrated DNA Technologies. ITS^+ (insulin, transferrin, and selenium), and Matrigel culture supplies were purchased from BD Biosciences. Unless otherwise specified, all cell culture reagents were purchased from Sigma-Aldrich or Invitrogen.

Culture and treatment of HPH. HPH were obtained from BioIVT. Hepatocytes with viability over 90% were seeded at 1.5×10^6, 7.5×10^5, or 3.75×10^5 cells/well in 6-, 12-, or 24-well collagen I–coated plates in INVITROGRO CP Medium (BioIVT). Twenty-four hours after seeding, HPH were overlaid with 0.25 mg/mL Matrigel in serum-free William's E Medium (WEM) (Sigma-Aldrich) supplemented with ITS^+, 0.1 μM dexamethasone (Sigma-Aldrich), 100 U/mL penicillin (ThermoFisher), 100 μg/mL streptomycin (ThermoFisher), and 2 mM L-glutamine (ThermoFisher) as described previously (15). Cultured HPH were treated with vehicle control (0.1% DMSO), RIF (10 μM), or CN06 at 1, 5, and 10 μM for 24 or 72 hours before harvesting cells for RNA and protein, respectively.

Culture and treatment of TNBC cells and CM. Human TNBC cell lines MDA-MB-231, HCC38, BT549, rat CM line H9c2, and human hepatocellular carcinoma line HepG2 cells were obtained from the American Tissue Culture Collection. The HepG2-CYP2B6-hCAR double stable cell line was generated as described previously (53) and cultured in DMEM (Thermo Fisher Scientific) supplemented with 10% FBS (ThermoFisher), 5 μg/mL blasticidin, 0.5 mg/mL geneticin, 100 U/mL penicillin, and 100 μg/mL streptomycin. MDA-MB-231, HepG2, and H9c2 cell lines were cultured in DMEM, and the BT549 and HCC38 cell lines were cultured in RPMI-1640 (Corning), containing 10% FBS and 100 U/mL penicillin and 100 μg/mL streptomycin in humidified incubator at 5% CO_2 and 37°C. Cultured cells were treated with a vehicle control (0.1% DMSO) or DOX (2.5 μM) in the presence and absence of CN06 (1 μM, 5 μM, 10 μM) for 24 hours before assessing viability and gene expression assays.

Culture and treatment of hiPSC-CM. hiPSC lines were generated from healthy subjects using an episomal approach and validated as described previously (54). Cardiac induction was achieved by small molecule delivery as described previously (55). In brief, at day 0, hiPSC were removed from mTeSR1 medium (Stemcell Technologies) and changed to supplemented RPMI 1640 (ThermoFisher) with B27 minus insulin (Invitrogen) and CHIR99021 (6 μM, Selleck Chemicals) for 48 hours. At day 2, medium was changed to RPMI 1640 with the addition of 2% B27 minus insulin for 3 days. At day 5, medium was changed to RPMI 1640 with 2% B27 minus insulin for 48 hours and changed every other day for 5 additional days. At day 10, medium was changed to RPMI 1640 with no glucose for 2 days and changed every other day for 6 days. At day 16, RPMI 1640 with 2% B27 complete (Invitrogen) with 100 U/mL penicillin and 100 μg/mL streptomycin was changed every other day following day 16 until day 30. hiPSC-CMs were treated with vehicle control (0.1% DMSO) or DOX (2.5 μM) in the presence and absence of CN06 at 1, 5, and 10 μM as indicated for analysis of cell viability and mRNA/protein expression.

Contractility assay. hiPSC-CMs (5×10^4) were seeded on Growth Factor Reduced Matrigel–coated (1:200 in DMEM/F-12) (Corning) 35 mm dishes (MatTek) with phenol free RPMI 1640, 2% B27 complete, 100 U/mL penicillin, and 100 μg/mL streptomycin. Cells were pretreated with vehicle control (0.1% DMSO) or CN06 (10 μM) for 24 hours, followed by treatment with DOX (1 μM) in the presence and absence of CN06 (10 μM) for 6 hours. Video-based edge detection was used to assess cellular shortening of the hiPSC-CMs during spontaneous contraction. hiPSC-CMs were visualized, and spontaneous contraction traces were recorded using a Nikon Ellipse coupled with IonOptix video microscopy system (IonOptix). Percent cell shortening values under each condition were averaged and analyzed using commercially available data analysis software (IonOptix, I IonWizzard v7.3). Nonshortening cells were excluded from analysis.

Immunocytochemistry analysis for hiPSC and hiPSC-CMs. OCT4 and TRA-60α were used for validation of hiPSCs and cardiac α-actinin for iPSC-CMs (Supplemental Table 3). For immunostaining, iPSCs and iPSC-CMs were fixed in 4% paraformaldehyde/PBS for 15 minutes at room temperature (RT), followed by

permeabilization with 0.2% TritonX-100 for 10 minutes. Specimens were blocked in goat-based blocking solution (Biogenix, HK112-9K) for 15 minutes at RT. Specimens were incubated with primary antibodies (detailed in Supplemental Table 3) diluted in the blocking solution at 4°C overnight. Fluorophore-conjugated secondary antibodies specific to the primary antibody IgG isotype were incubated for 1 hour in the dark at RT. VectaShield (Vector Labs) was mounted after thoroughly washing with 0.2% TritonX-100 in PBS. Specimens were visualized using a Nikon A1 point-scanning laser confocal microscope.

Quantitative HTS assays. HepG2-CYP2B6-hCAR cells in culture medium without geneticin and blasticidin were dispensed at 2500 cells/4 μL/well into white wall/solid bottom, tissue culture–treated 1536-well plates (Greiner Bio-One North America) using a Multidrop Combi (Thermo Fisher Scientific). After an incubation at 37°C/5% CO_2 for 5 hours, 23 nL of vehicle control (0.1% DMSO), test compounds, or the positive control (CITCO; Sigma-Aldrich) were transferred to the assay plates by a Wako Pintool station (Wako Automation). PK11195 (Sigma-Aldrich), a known CAR antagonist (56), was then added (1 μL) to generate a final concentration of 0.75 μM in each well using a BioRAPTR Flying Reagent Dispenser (FRD; Beckman Coulter). A total of 5632 structurally unique compounds from the NPACT library and 277 compounds from a UMB library each with 7 concentrations were screened. The concentrations are in a 1:5 dilution starting with 10 mM, 6.7 mM, or 5 mM depending on the solubility of each compound. After an incubation at 37°C/5% CO_2 for 24 hours, 4 μL of ONE-Glo Luciferase reagent (Promega) was added to each well using the BioRAPTR FRD. After a 30-minute incubation at RT, luminescence intensity was measured using the ViewLux plate reader (Perkin Elmer). Data were then expressed in relative luminescence units, and analysis was done as described previously (24).

For quantitative Nrf2/ARE β-lactamase reporter experiment, CellSensor ARE-*bla* HepG2 cells (Thermo Fisher Scientific) in assay medium (DMEM with GLutaMAX containing 1% dialyzed FBS, 0.1 mM nonessential amino acids (Sigma-Aldrich), 25 mM HEPES (Sigma-Aldrich), and 100 U/mL penicillin, and 100 μg/mL streptomycin) were cultured and assayed as described previously (25).

Ad/EYFP-hCAR translocation assay. Twenty-four hours after seeding, HPH were infected with Ad/EYFP-hCAR at a concentration of 5 μL/mL in complete WEM and incubated overnight (57). HPH-infected cells were treated with a vehicle control (0.1% DMSO), a positive control (1 mM PB), and CN06 (10 μM) for 8 hours. Following the treatment, cells were fixed in 4% paraformaldehyde for 15 minutes, and DAPI was added (1:1000) in PBS for 30 minutes. Fluorescence was viewed using the YFP/FITC and the DAPI channel (Nikon Eclipse Ti) and quantified by identifying the number of cells expressing EYFP-hCAR present in the nucleus over the total cells expressing EYFP-hCAR (n = 300). Representative images are shown, and quantitative data represent the mean ± SD of 3 images, 100 cells per image, for each treatment.

Multicellular cocultures. HPH, seeded in collagen I–coated 24-well plates or 6-well plates, were pretreated with vehicle control (0.1% DMSO) or CN06 (10 μM) for 24 hours. BT549 and H9c2 cells were seeded on 2 separate collagen I–coated coverslips modified to have their corners bent and allowed 24 hours for attachment. Following the 24-hour pretreatment, coverslips with BT549 and/or H9c2 rat CM were inserted in HPH-seeding wells as depicted in Figure 2H and Figure 6A. Cocultured cells were exposed to designated concentrations of CPA or a combination of CPA/DOX in the presence or absence of CN06 (10 μM) for 24–72 hours at 37°C with 5% CO_2. BT549 and H9c2 cells were harvested and assessed for viability, apoptosis, and DNA damage. Cell culture medium was collected for LC-MS/MS analysis of CPA and 4-OH-CPA as detailed below.

Reverse transcription PCR (RT-PCR). Total RNA was isolated from treated cells using the TRIzol reagent (Thermo Fisher Scientific) and reverse transcribed to cDNA using a High-Capacity cDNA Archive kit (Applied Biosystems) according to the manufacturer's instructions. PCR was performed on an ABI StepOnePlus Real-Time PCR system (Applied Biosystems) using Fast SYBR Green Master Mix (Qiagen) to determine gene expression changes. Primer sequences for CYP2B6, CYP3A4, HO-1, Nrf2, and GAPDH include the following: CYP2B6, (forward) 5′-AGACGCCTTCAATCCTGACC-3′ and (reverse) 5′-CCTTCACCAAGACAAATCCGC-3′; CYP3A4, (forward) 5′-GTGGGGCTTTTATGATGGTCA-3′ and (reverse) 5′-GCCTCAGATTTCTCACCAACACA-3′; HO-1, (forward) 5′-GGGTGATAGAAGAGGCCAAGACT-3′ and (reverse) 5′-AGCTCCTGCAACTCCTCAAAG-3′; NRF2, (forward) 5′-TCAGCGACGGAAAGAGATATGA-3′ and (reverse) 5′-CCACTGGTTTCTGACTGGATGT-3′; and GAPDH, (forward) 5′-CCCATCACCATCTTCCAGGAG-3′ and (reverse) 5′-GTTGTCATGGATGACCTTGGC-3′. Relative expression values were quantified using the equation: fold over control = $2^{\Delta\Delta Ct}$ method, where ΔCt represents the differences in cycle threshold numbers between the target gene and GAPDH as the housekeeping gene, and ΔΔCt is the relative change in these differences between control and treatment groups.

Immunoblotting. Homogenized protein (20–30 μg) from whole cell or nuclear and cytosol, extracted using ChIP-IT Express Kit (Active Motif), from treated cells were resolved on NuPage Novex Bis-Tris 4%–12% gels (Invitrogen) or 12% gel and transferred through electrophoresis onto polyvinylidene difluoride (PVDF) membranes. Membranes were blocked at 5% BSA (Research Product International [RPI]) or 5% Blocker (Bio-Rad) for 1 hour at RT. Furthermore, membranes were incubated overnight with primary antibodies at 4°C followed by secondary antibody for 1 hour at RT (Supplemental Table 3). Membranes were incubated in SuperSignal West Pico Chemiluminescent Substrate (Thermo Fisher Scientific) or Radiance Q (Azure) and imaged using C300 (Azure). ImageJ (NIH) was used for quantitation from 3 separately prepared cell experiments and normalized to the density of the loading control.

Cell viability assay. H9c2 rat CM (0.8×10^5 cells/well), TNBC cells (1×10^5 cells/well), and hiPSC-CMs (1×10^6 cells/well) were seeded in 24-well plates and cultured for 24 hours in 37°C and 5% CO_2. A 2 hour pretreatment with a vehicle control (0.1% DMSO) or CN06 (1 μM, 5 μM, or 10 μM) was followed by a cotreatment with ranging concentrations of DOX (2.5 μM) for 22 hours. In a separate experiment, coculture cells were assembled and treated with CPA and DOX in the presence and absence of CN06 (10 μM) as indicated. A Cell Counting Kit-8 (CCK-8, Enzo) assay was carried out based on the manufacturer's instructions. In brief, cell viability was quantified by measuring the conversion of the WST-8 substrate to formazan, driven by dehydrogenases in cells, and this conversion is directly proportional to the number of living cells. Cell viability was calculated as a percent of vehicle control (0.1% DMSO) using a SpectraMax M5 microplate reader (Molecular Devices). Additionally, a Cell-Titer Glo luminescent cell viability assay (Promega) was utilized to validate some of the CCK-8 experiment data. This assay determines the number of viable cells in culture based on quantitation of the ATP, which signals the presence of metabolically active cells.

LC-MS/MS determination of 4-OH-CPA formation. Following a 24-hour pretreatment of a vehicle control (0.1% DMSO) or CN06 (10 μM) with CPA (250 μM, 500 μM, 1000 μM), 200 μL of cell culture medium was removed from each treatment group and immediately mixed with 20 μL of SCZ (2M) to stabilize 4-OH-CPA to its derivative 4-OH-CPA–SCZ. Sample preparation and LC-MS/MS analysis was conducted as described previously (43). The mass spectrometer and the selected reaction monitoring (SRM) mode for CPA and 4-OH-CPA detection was performed on an Acquity UPLC BEHC8 (50 mm x 2.1 mm, 1.7 μM) column, with the mobile phase consisting of 100:0.1 water/formic acid and 100:0.1 acetonitrile/formic acid.

Phosphorylated H2AX imaging. The H9c2 rat CM and BT549 cells seeded on modified coverslips were removed from the treated multicellular cocultures. Cells were fixed in 4% paraformaldehyde in PBS, permeabilized, and incubated with primary mouse anti–phospho-H2AX (Supplemental Table 3) as described previously (8). Nuclear DNA was stained using DAPI at 1 μg/mL. The coverslips were visualized at 10× magnification using fluorescence microscopy (Nikon Eclipse Ti), and the amount of phosphorylation was quantified as mean integrated intensity using bright-spot detection from 3 whole wells and normalized to the vehicle control (0.1% DMSO).

ROS measurement. H9c2 rat CM seeded at 0.8×10^5 cells/well in 24-well plates while BT549 and MDA-MB-231 cells were seeded at 1×10^5 cells/well. All cells were pretreated with vehicle control (0.1% DMSO) or CN06 (10 μM) for 2 hours and cotreated with DOX (1 μM, 2.5 μM, and 5 μM) for 6 hours. Subsequently, 0.5 mL of WEM containing 20 μM DFDA or 5 μM of Cell Rox Green Reagent (Thermo Fisher Scientific) was added to each well. Concurrently, Hoechst (Thermo Fisher Scientific) was added at 10 μg/mL for 1-hour incubation. The oxidation of the fluorescent probe was viewed at 10× magnification using fluorescence microscopy (Nikon Eclipse Ti) and quantified using NIS-Element Analysis with bright-spot detection to get mean integrated intensities from 3 whole-well images and normalized to the vehicle control (0.1% DMSO).

Statistics. All statistical analyses were performed using GraphPad Prism's (v.7). Significance across the mean values of each triplicated group was done using 2-tailed *t* test for 2 experimental groups. For comparison with at least 3 groups, 1-way ANOVA with Dunnett's or Bonferroni analysis or 2-way ANOVA with Bonferroni analysis was used to assess overall differences among groups. Results are shown as mean ± SD. $P < 0.05$ was considered significant..

Study approval. hiPSC lines were generated from healthy control subjects using an episomal approach under protocols approved by the Vanderbilt University IRB and validated previously (54, 55, 58).

Author contributions

S. Stern, LL, CCH, FX, and HW participated in research design. S. Stern, LL, DL, RK, S. Sakamuru, KAK, CL, and SH conducted experiments. MX, JZ, CCH, and SH contributed new reagents or analytic tools. S. Stern, LL, CL, RH, YWC, FX, and HW performed data analysis. S. Stern, LL, CL, MX, JZ, YWC, CCH, FX, and HW wrote or contributed to the writing of the manuscript.

Acknowledgments

This work was partly supported by the NIH (grants GM121550 and CA262084), the Maryland Innovation Initiative (MII), and the Intramural Research Program of the NCATS. S. Stern is a predoctoral fellow supported by the UMB, Institute for Clinical & Translational Research, which is funded by the Clinical and Translational Science Award with a trainee grant, 1UL1TR003098-01. RK was partly supported by the University of Maryland's Center of Excellence in Regulatory Science and Innovation (M-CERSI) Scholars Program funded by the FDA (2U01FD0059462). We appreciate Jean-Pierre Raufman for critical reading of the manuscript. We thank Carleen Klumpp-Thomas from NCATS for compound screening support, and BioIVT for providing HPH for this study.

Address correspondence to: Hongbing Wang or Fengtian Xue, Department of Pharmaceutical Sciences, University of Maryland School of Pharmacy, 20 Penn Street, Baltimore, Maryland 21201, USA. Phone: 410.706.1280; Email: hongbing.wang@rx.umaryland.edu (HW). Phone: 410.706.8521; Email: fxue@rx.umaryland.edu (FX).

1. Siegel RL, et al. Cancer statistics, 2022. *CA Cancer J Clin*. 2022;72(1):7–33.
2. Oakman C, et al. Management of triple negative breast cancer. *Breast*. 2010;19(5):312–321.
3. Wahba HA, El-Hadaad HA. Current approaches in treatment of triple-negative breast cancer. *Cancer Biol Med*. 2015;12(2):106–116.
4. Zeichner SB, et al. A review of systemic treatment in metastatic triple-negative breast cancer. *Breast Cancer (Auckl)*. 2016;10:25–36.
5. Buyukhatipoglu H, et al. A retrospective analysis of adjuvant CAF, AC-T and TAC regimens in triple negative early stage breast cancer. *J BUON*. 2015;20(1):22–27.
6. Bonadonna G, et al. Adjuvant cyclophosphamide, methotrexate, and fluorouracil in node-positive breast cancer: the results of 20 years of follow-up. *N Engl J Med*. 1995;332(14):901–906.
7. Fenselau C, et al. Identification of aldophosphamide as a metabolite of cyclophosphamide in vitro and in vivo in humans. *Cancer Res*. 1977;37(8 pt 1):2538–2543.
8. Hedrich WD, et al. Activation of the constitutive androstane receptor increases the therapeutic index of CHOP in lymphoma treatment. *Mol Cancer Ther*. 2016;15(3):392–401.
9. Huang Z, et al. Role of human liver microsomal CYP3A4 and CYP2B6 in catalyzing N- dechloroethylation of cyclophosphamide and ifosfamide. *Biochem Pharmacol*. 2000;59(8):961–972.
10. Code EL, et al. Human cytochrome P4502B6: interindividual hepatic expression, substrate specificity, and role in procarcinogen activation. *Drug Metab Dispos*. 1997;25(8):985–993.
11. Roy P, et al. Development of a substrate-activity based approach to identify the major human liver P-450 catalysts of cyclophosphamide and ifosfamide activation based on cDNA-expressed activities and liver microsomal P-450 profiles. *Drug Metab Dispos*. 1999;27(6):655–666.
12. Hedrich WD, et al. Insights into CYP2B6-mediated drug-drug interactions. *Acta Pharm Sin B*. 2016;6(5):413–425.
13. Mackowiak B, et al. The roles of xenobiotic receptors: beyond chemical disposition. *Drug Metab Dispos*. 2018;46(9):1361–1371.
14. Wang D, et al. The constitutive androstane receptor is a novel therapeutic target facilitating cyclophosphamide-based treatment of hematopoietic malignancies. *Blood*. 2013;121(2):329–338.
15. Faucette SR, et al. Differential regulation of hepatic CYP2B6 and CYP3A4 genes by constitutive androstane receptor but not pregnane X receptor. *J Pharmacol Exp Ther*. 2006;317(3):1200–1209.
16. Bai Y, et al. Sulforaphane protection against the development of doxorubicin-induced chronic heart failure is associated with Nrf2 upregulation. *Cardiovasc Ther*. 2017;35(5).
17. Renu K, et al. Molecular mechanism of doxorubicin-induced cardiomyopathy — an update. *Eur J Pharmacol*. 2018;818:241–253.
18. Timm KN, Tyler DJ. The role of AMPK activation for cardioprotection in doxorubicin-induced cardiotoxicity. *Cardiovasc Drugs Ther*. 2020;34(2):255–269.
19. Sterba M, et al. Oxidative stress, redox signaling, and metal chelation in anthracycline cardiotoxicity and pharmacological cardioprotection. *Antioxid Redox Signal*. 2013;18(8):899–929.
20. De la Vega MR, et al. NRF2 and the hallmarks of cancer. *Cancer Cell*. 2018;34(1):21–43.
21. Kwak MK, Kensler TW. Targeting NRF2 signaling for cancer chemoprevention. *Toxicol Appl Pharmacol*. 2010;244(1):66–76.
22. Masahiko N, Honkakoski P. Induction of drug metabolism by nuclear receptor CAR: molecular mechanisms and implications for drug research. *Eur J Pharm Sci*. 2000;11(4):259–264.
23. Tonelli C, et al. Transcriptional regulation by Nrf2. *Antioxid Redox Signal*. 2018;29(17):1727–1745.
24. Lynch C, et al. Quantitative high-throughput identification of drugs as modulators of human constitutive androstane receptor. *Sci Rep*. 2015;5:10405.
25. Zhao J, et al. Cell-based assay for identifying the modulators of antioxidant response element signaling pathway. *Methods Mol*

Biol. 2016;1473:55–62.
26. Liang D, et al. Human constitutive androstane receptor agonist DL5016: a novel sensitizer for cyclophosphamide-based chemotherapies. *Eur J Med Chem*. 2019;179:84–99.
27. Wang H, LeCluyse EL. Role of orphan nuclear receptors in the regulation of drug-metabolising enzymes. *Clin Pharmacokinet*. 2003;42(15):1331–1357.
28. Faucette SR, et al. Relative activation of human pregnane X receptor versus constitutive androstane receptor defines distinct classes of CYP2B6 and CYP3A4 inducers. *J Pharmacol Exp Ther*. 2007;320(1):72–80.
29. Moore LB, et al. Orphan nuclear receptors constitutive androstane receptor and pregnane X receptor share xenobiotic and steroid ligands. *J Biol Chem*. 2000;275(20):15122–15127.
30. Li H, Wang H. Activation of xenobiotic receptors: driving into the nucleus. *Expert Opin Drug Metab Toxicol*. 2010;6(4):409–426.
31. Li H, et al. Nuclear translocation of adenoviral-enhanced yellow fluorescent protein-tagged-human constitutive androstane receptor (hCAR): a novel tool for screening hCAR activators in human primary hepatocytes. *Drug Metab Dispos*. 2009;37(5):1098–1106.
32. Li L, et al. Differential activation of pregnane X receptor and constitutive androstane receptor by buprenorphine in primary human hepatocytes and HepG2 cells. *J Pharmacol Exp Ther*. 2010;335(3):562–571.
33. Lynch C, et al. Identification of novel activators of constitutive androstane receptor from FDA-approved drugs by integrated computational and biological approaches. *Pharm Res*. 2013;30(2):489–501.
34. Furfaro AL, et al. The Nrf2/HO-1 axis in cancer cell growth and chemoresistance. *Oxid Med Cell Longev*. 2016;2016:1958174.
35. Havelka AM, et al. Mechanisms of action of DNA-damaging anticancer drugs in treatment of carcinomas: is acute apoptosis an "off-target" effect? *Mini Rev Med Chem*. 2007;7(10):1035–1039.
36. Pereira-Oliveira M, et al. Doxorubicin is key for the cardiotoxicity of FAC (5-fluorouracil + Adriamycin + cyclophosphamide) combination in differentiated H9c2 cells. *Biomolecules*. 2019;9(1):E21.
37. Govender J, et al. Melatonin improves cardiac and mitochondrial function during doxorubicin-induced cardiotoxicity: a possible role for peroxisome proliferator-activated receptor gamma coactivator 1-alpha and sirtuin activity? *Toxicol Appl Pharmacol*. 2018;358:86–101.
38. Kim SY, et al. Doxorubicin-induced reactive oxygen species generation and intracellular Ca2+ increase are reciprocally modulated in rat cardiomyocytes. *Exp Mol Med*. 2006;38(5):535–545.
39. Kuo LJ, Yang LX. Gamma-H2AX — a novel biomarker for DNA double-strand breaks. *In Vivo*. 2008;22(3):305–309.
40. Pass GJ, et al. Role of hepatic cytochrome p450s in the pharmacokinetics and toxicity of cyclophosphamide: studies with the hepatic cytochrome p450 reductase null mouse. *Cancer Res*. 2005;65(10):4211–4217.
41. Ma J, Waxman DJ. Modulation of the antitumor activity of metronomic cyclophosphamide by the angiogenesis inhibitor axitinib. *Mol Cancer Ther*. 2008;7(1):79–89.
42. De Giorgi U, et al. High-dose chemotherapy for triple negative breast cancer. *Ann Oncol*. 2007;18(1):202–203.
43. Kurian R, et al. CITCO as an adjuvant facilitates CHOP-based lymphoma treatment in hCAR-transgenic mice. *Cells*. 2020;9(11):E2520.
44. Octavia Y, et al. Doxorubicin-induced cardiomyopathy: from molecular mechanisms to therapeutic strategies. *J Mol Cell Cardiol*. 2012;52(6):1213–1225.
45. Bose C, et al. Sulforaphane potentiates anticancer effects of doxorubicin and attenuates its cardiotoxicity in a breast cancer model. *PLoS One*. 2018;13(3):e0193918.
46. Hu X, et al. miR-200a attenuated doxorubicin-induced cardiotoxicity through upregulation of Nrf2 in mice. *Oxid Med Cell Longev*. 2019;2019:1512326.
47. Hedrich WD, Wang H. Friend or foe: xenobiotic activation of Nrf2 in disease control and cardioprotection. *Pharm Res*. 2021;38(2):213–241.
48. Taguchi K, et al. Molecular mechanisms of the Keap1–Nrf2 pathway in stress response and cancer evolution. *Genes Cells*. 2011;16(2):123–140.
49. Ballan N, et al. Single-cell mechanical analysis of human pluripotent stem cell-derived cardiomyocytes for drug testing and pathophysiological studies. *Stem Cell Reports*. 2020;15(3):587–596.
50. Sharma A, et al. High-throughput screening of tyrosine kinase inhibitor cardiotoxicity with human induced pluripotent stem cells. *Sci Transl Med*. 2017;9(377):eaaf2584.
51. Davis J, et al. In vitro model of ischemic heart failure using human induced pluripotent stem cell-derived cardiomyocytes. *JCI Insight*. 2021;6(10):e134368.
52. Zang H, et al. The dark side of Nrf2 in the heart. *Front Physiol*. 2020;11:722.
53. Lynch C, et al. Quantitative high-throughput luciferase screening in identifying CAR modulators. *Methods Mol Biol*. 2016;1473:33–42.
54. Chun YW, et al. Combinatorial polymer matrices enhance in vitro maturation of human induced pluripotent stem cell-derived cardiomyocytes. *Biomaterials*. 2015;67:52–64.
55. Feaster TK, et al. Matrigel mattress: a method for the generation of single contracting human-induced pluripotent stem cell-derived cardiomyocytes. *Circ Res*. 2015;117(12):995–1000.
56. Li L, et al. The peripheral benzodiazepine receptor ligand 1-(2-chlorophenyl-methylpropyl)-3-isoquinoline-carboxamide is a novel antagonist of human constitutive androstane receptor. *Mol Pharmacol*. 2008;74(2):443–453.
57. Mackowiak B, Wang H. High-content analysis of constitutive androstane receptor nuclear translocation. *Methods Mol Biol*. 2019;1966:71–77.
58. Cadar AG, et al. Real-time visualization of titin dynamics reveals extensive reversible photobleaching in human induced pluripotent stem cell-derived cardiomyocytes. *Am J Physiol Cell Physiol*. 2020;318(1):C163–C173.